Narrow-Band QD-Enhanced PIN Metal-Oxide Heterostructure Phototransistor with the Assistance of Printing Processes

Xiang Liu, Wenxing Zhou, Yuan Tao, Lei Mao, Jianhua Chang, Hai Hu, Chi Li,* and Qing Dai**

Infrared (IR) phototransistors are important building blocks for the true integration of flat-panel optoelectronic detectors. Although significant progress is made in obtaining an InGaZnO active layer with IR response, the utilization of a high-performance detector still has many challenges due to low efficiency, high power consumption, and lagging detection speed. Herein, a positive-intrinsic-negative (PIN) heterostructure phototransistor directly modulating the charges' transfer barrier with low power consumption (1 nW), high efficiency (EQE > 700%), a 200 Hz detecting bandwidth, and high detectivity (1×10^{11} cm $Hz^{1/2}$ W^{-1}) at an IR wavelength (1.5 μm in the high-frequency circumstance) is demonstrated. These excellent sensing properties of the PIN phototransistor, together with its advantages of low power consumption and versatility, make the use of a heterostructure a powerful strategy for the development of on-chip optoelectronic detectors.

Indium gallium zinc oxide (IGZO) phototransistors associated with quantum dots (QDs) and other low-dimensional materials have attracted intense research interest because they are stable and high-performance electronic systems with unique efficient optoelectric properties.[1–4] To date, the IGZO active layer has provided low modulated gate voltage, low subthreshold swing (SS), high on–off ratios and other electric properties for phototransistors.[5,6] QDs and low-dimensional materials can produce a high optoelectric conversion efficiency and rate, low dark current, high responsivity and detectivity for the phototransistor as a high-performance integrated detector.[7–11] However, key obstacles to their wide range of use in integrated-photodetection applications must urgently be addressed. For example, the wide-band semiconductor nature of IGZO leads to a low efficiency in the infrared waveband,[12] the persistent photoconductivity (PPC) effect results in slow recovery of the photocurrent,[13] and the hybrid sensing structure gives rise to a tradeoff between the long carrier lifetimes and the demand for rapid detection.[14]

In-depth studies on heterostructure photodetectors are of particular interest because this approach can boost the optoelectric conversion efficiency.[15,16] In particular, the QD-based PIN structure detector with both electron and hole blockers show low dark current, sensitive light absorption and high detectivity due to its enhanced structure.[17–19] Otherwise, appropriate Schottky junctions and other heterojunctions have been reported to decrease the device driving power and increase the detection performances in IGZO-based phototransistor.[2,20–22] Although the additional photocarriers provide substantial benefits and great potential for applications, the developments of PIN heterostructures combined with a phototransistor are still rarely reported. In our previous work, we have demonstrated the high efficiency planar and vertical phototransistor combined with both optoelectric conversion and light signal reading out with a hybrid light-sensing channel.[23,24]

We further found that the vertically stacked PIN such as the QD IR phototransistor with a charge-blocking layer can exhibit outstanding optoelectric properties (high efficiency, responsivity, detectivity, and so on) and excellent electric performance characteristics (low driving power, gate voltage, and so on). In particular, due to the negative bandgap (–0.3 eV) of the topological insular HgTe[25] and direct bandgap of CdTe (1.7 eV), the PIN heterostructure composed of these materials has tremendous potential for use in any infrared (IR) waveband. In this letter, we describe ternary compound semiconductor QDs (CdHgTe, mercury telluride, mercury cadmium tellurium (MCT) QDs) adopted as the optoelectric conversion core that can provide high light-absorption and sensitivity in IR-detecting applications.[26,27] These characteristics motivate us to investigate the performance of the phototransistor with the assistance of an inkjet and dispensing printing process that can simplify the formation and alignment of the heterostructures. Due to its high photocurrent gain, low dark current and low operating voltage, the PIN phototransistor exhibits a high external quantum efficiency (EQE) (700%) at a low working electric power of 1 nW and a high detectivity value of 1×10^{11} Jones

Dr. X. Liu, W. Zhou, Y. Tao, L. Mao, Prof. J. Chang
School of Electronics and Information Technology
Nanjing University of Information Science and Technology
Nanjing 210096, China
Prof. H. Hu, Prof. C. Li, Prof. Q. Dai
CAS Center for Excellence in Nanoscience
National Center for Nanoscience and Technology
Beijing 10010, China
E-mail: lichi@nanoctr.cn; daiq@naoctr.cn
Prof. H. Hu
University of Chinese Academy of Sciences
Beijing 10049, China
E-mail: Huh@nanoctr.cn

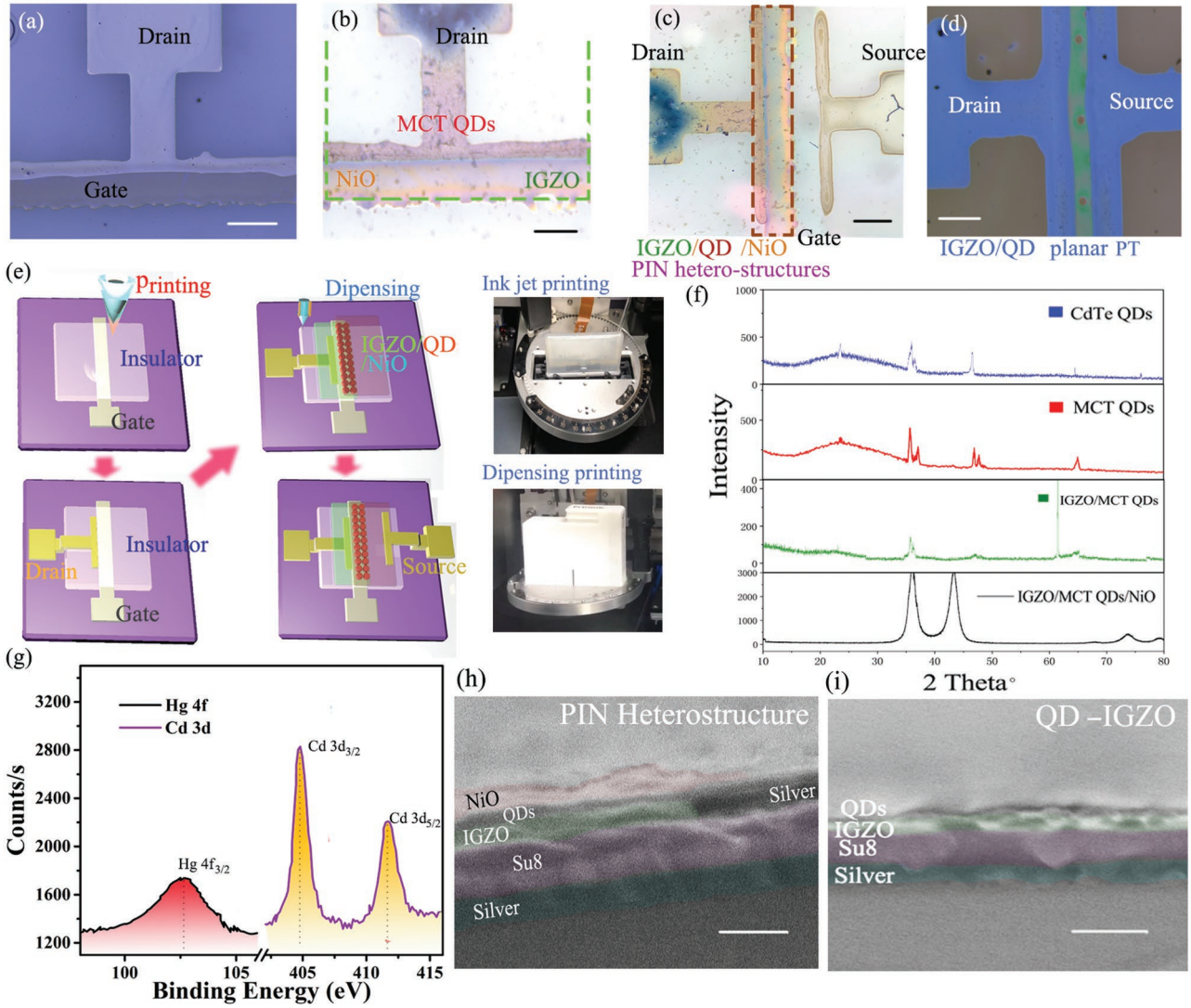

Figure 1. a) Top-view microscope image of gate electrode/insulator/drain electrode fabricated by inkjet printing (scale bar: 150 µm). b) Optical microscope image of the device with metal-oxide and QD active layers fabricated by intrinsic dispensing printing processes (scale bar: 150 µm). c) Overall image of the completed PIN heterostructure phototransistor (scale bar: 200 µm). d) The contrasted planar phototransistor with IGZO/QD photosensing components in the channel (scale bar: 150 µm). e) Schematics of the as-fabricated phototransistor's production processes. X-ray diffraction (XRD) f) and X-ray photoelectron spectroscopy (XPS) spectra of the metal-oxide components g), QDs and the hybrids. SEM cross-sectional images (scale: 400 nm) of the PIN heterostructure h) and QD-IGZO phototransistors i).

under an IR wavelength (1.5 µm) that is comparable to that of a commercial III–IV photodetector.

The schematic diagrams of the proposed device's fabrication processes are illustrated in **Figure 1**a–e, representing the two specific architectures of the IGZO phototransistors. For this PIN phototransistor, the bottom-gate field effect transistor with the top-contact electrode are produced as follows: silver Ag ion ink and Su8 2000.5 thin film insulator ink were jetted using a drop-on-demand piezoelectric IJP system (multifunctional scientific printing machine, Shanghai Prtronic Ltd.) with a 25 µm nozzle at a pulse of 1000 Hz in ambient conditions with Ag/Su8/Ag (200/500/200 nm) vertical structures, as shown in the top-view optical and cross-sectional scanning electron microscope (SEM) images of Figure 1a,h. The IGZO solution was prepared by mixing 1.0 M zinc acetate dehydrate [$Zn(CH_3COO)_2 \cdot 2H_2O$, 99.99%], 0.5 M gallium nitrate hydrate [$Ga(NO_3)_3 \cdot H_2O$], and 0.5 M indium nitrate hydrate [$In(NO_3)_3 \cdot H_2O$, 99.99%] in 2-methoxyethanol solvent. The solution was added to a stabilizer and stirred for 3 h at 50 °C, and then the collected IGZO solution was jetted by an air injection dispensing system of the printing machine with a 35 kPa and 300 µm nozzle. Compared with piezoelectric injection, the air injection dispensing printing process has low ink quality and substrate flatness demands (as illustrated in the atomic force microscope (AFM) images of every layer), which adapts to relatively low precision, multilayer and cost-effective semiconductor formation.[28] Finally, the rapid laser annealing process (with an excimer XeCl 308 nm laser ultraviolet source with

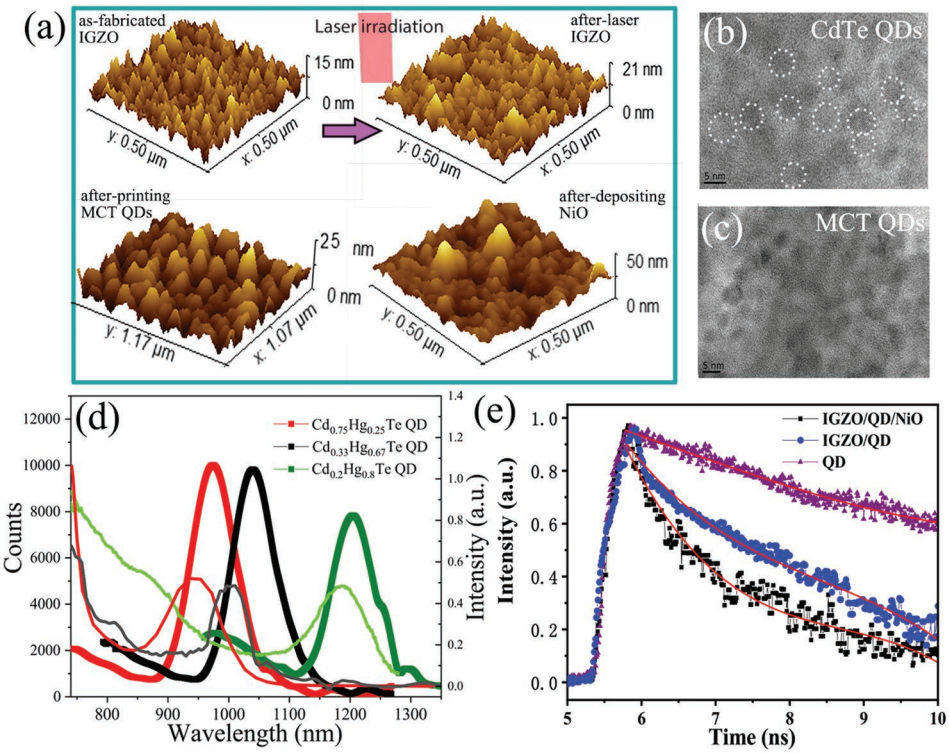

Figure 2. a) AFM images of the deposited IGZO, after-laser IGZO, MCT QDs, and NiO by the printing process. HRTEM images for the CdTe QDs' b) and MCT QDs' c) morphologies. d) PL and absorption spectra of MCT QDs with different Hg ratios. e) Time resolved photoluminescence (TRPL) measurements for the deposited layers with different components.

300 mJ cm^{-2}) was used to improve the active layer's quality, where more granules emerged and can be observed in the AFM image in **Figure 2**a.

To demonstrate the high quality of the MCT QDs, high resolution transmission electron microscope (HRTEM) images of the original CdTe QDs and MCT QDs are shown in Figure 2b,c. MCT QDs are synthesized from a commercial CdTe QDs precursor aqueous solution through cation exchange with a N_2 gas flow. Because Cd^{2+} and Hg^{2+} have similar properties (II B group elements, as illustrated in XPS datas of Figure 1g), this cation exchange method[29,30] can modulate the photoluminescence (PL) and absorption characteristics without altering the diameters of the QDs. Compared with CdTe QDs with a well-defined lattice structure, the MCT QDs' lattice images became unclear after the exchange process, as illustrated in Figure 2b,c. However, remarkably, the reaction ratio of the Hg^{2+} to Cd^{2+} exchange can lead to the redshift of the PL and absorption peaks (Figure 2d).

Furthermore, the MCT QD aqueous dispersion and NiO solution were also deposited on the IGZO thin film to form the PIN (NiO/QD/IGZO) heterostructures using an air injection dispensing system. A commercial NiO nanoparticle (30 nm diameter) toluene solution was purchased as the dispensing ink at 25 kPa and with a 300 μm nozzle. Figure 1f shows the XRD patterns of the separated layers with different combinations for which the hybrid components' information can be clearly observed. The additional top-aligned silver electrode is formed on the NiO layer through the inkjet printing process.

The TRPL traces are representative of the transient evolution of e–h generation and transfer after pulsed photoexcitation, as shown in Figure 2e. The carrier lifetime of the IGZO/QD/NiO heterostructure (0.23 ns) is shorter than that of IGZO/QD (0.3 ns) and is approximately two times shorter than that of pristine QDs (0.52 ns). This is because zinc oxide-based IGZO is a typical electron transport material (ETL) and hole blocking layer (HBL), while NiO is a classic hole transport material (HTL) and electron blocking layer (EBL). These two layers can extract electrons and holes, respectively, and give rise to a dramatic carrier quenching effect that is beneficial for obtaining a high-performance photodetector. In addition, the QD/IGZO hybrid channel phototransistor (PT) and NiO/QD/IGZO heterostructure phototransistor were also fabricated for comparison in order to study the mechanism of this PIN structure and its impact on the performance characteristics.

In the present experiments, we revisited the electronic characterizations in the dark and under different operational gate voltages. **Figure 3**a shows the I_{DS}–V_{DS} output characteristic measurements of the PIN phototransistor obtained with the four-probe station and semiconductor analyzer (HP 4156B). Current, I_{DS}, flows from the n-type IGZO (drain) to the p-type NiO (source), and the voltage is applied across the IGZO/QD/NiO heterostructure only, yielding a rectification for the output characteristic curves, as shown in Figure 3e. Another key phenomenon that affects the performances of the PIN phototransistor is that the transistor should have better modulation capability in the positive terminal, which has an obvious cutoff region at reverse bias. Meanwhile, the output characteristics of conventional QD/IGZO PT exhibit equilibrium ambipolar properties for both positive and negative bias V_{DS}. This can also

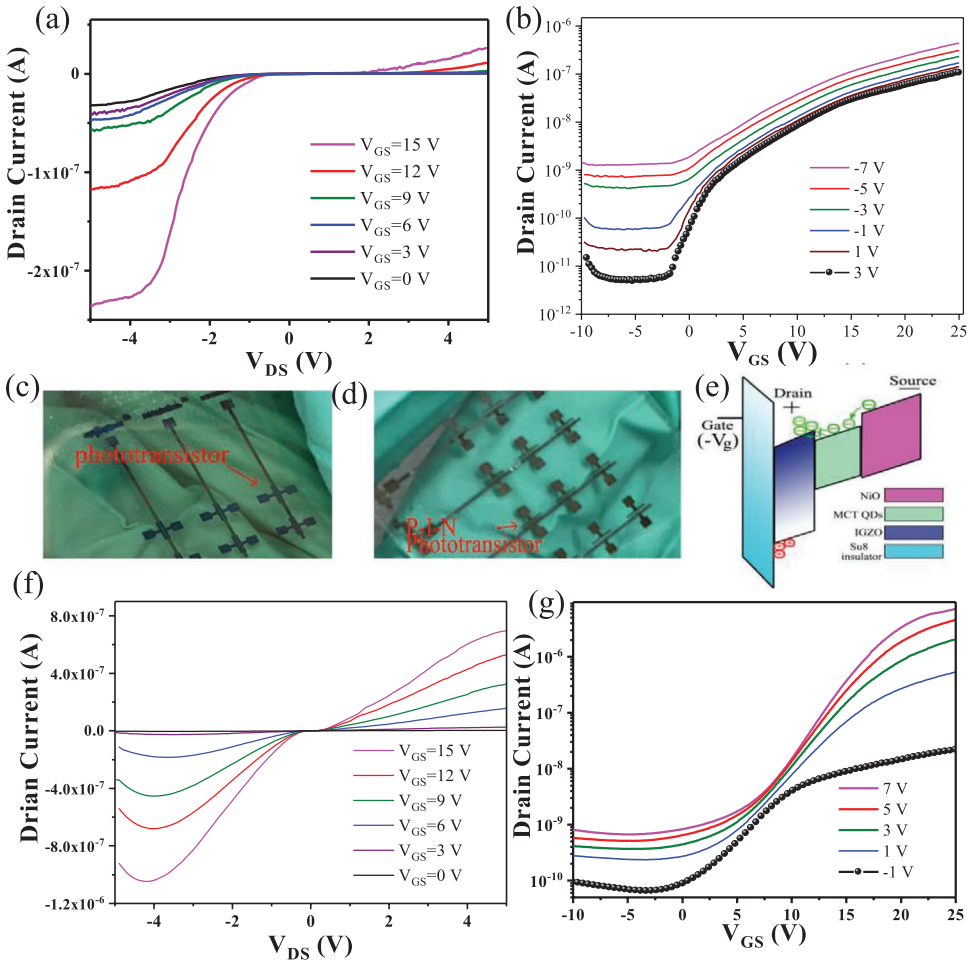

Figure 3. a) Output characteristic curves for the PIN phototransistor. b) Transfer characteristic curves of the PIN phototransistor. Images obtained for the conventional PT c) and the PIN phototransistor devices d). e) Charge transfer mechanism of the PIN phototransistor at the off-state. f) Output characteristic curves for the QD-IGZO PT. g) Transfer characteristic curves of IGZO/QD PT in the dark.

be identified by the transfer characteristics under previous specific V_{DS}. The on/off ratio and electric property deterioration is due to the lack of a cutoff region prior to the as-constructed PIN heterostructure, as indicated by the data presented in Figure 3b.

Figure 3e shows the carrier transfer within the PIN heterostructure of the drain–source terminals and heterostructure transistor's operating mechanism[31,32] under the dark state. When the gate is applied by the negative bias, the holes are drawn to the IGZO/insulator interface and electrons are induced to move toward the IGZO/QD terminal. This procedure not only blocks hole's injection into QD layer but also increases the electron transfer barrier from the source to the IGZO drain terminal. By contrast, the dark current of the conventional PT shows fewer effects of the variation of V_{DS}, as demonstrated in Figure 3g. There is a close correspondence between the transfer and output characteristics based on the different operation mechanisms.

The two transfer characteristics shown in Figure 3b,g correspond to two operation modes of the phototransistor with IGZO as the active layer. Because the organic Su8 insulator is thick and has many defects in contact with the inorganic IGZO active layer, it exhibits poor SS (1.7 V decade^{-1}), a high threshold operated gate voltage (V_{GS} = 12 V), and a high driving drain voltage (>3 V). More than 50 such PIN phototransistors were fabricated, showing 0.87 V decade^{-1}, 5 V threshold gate voltage and low drain voltage (<1 V) at room temperature. Consequently, building an efficient heterostructure inside the channel may be an alternative approach to improving either the solution-process or printing phototransistor's quality, because this usually requires the use of an aqueous phase insulator ink. Additionally, this structure shows potential for achieving a high-performance phototransistor with reduced supplied power.

The photoresponse of the PIN phototransistor shows a noticeable enhancement when light with different wavelengths is introduced into the channel, as shown in **Figure 4**a. The structure-divisive charge transfer efficiency accounts for the control of the screening and extraction of the photosensing core, as illustrated in Figure 4. Compared with the above-described charge transfer under the dark state and negative off-gate voltage, the enhanced separated photoexcited carriers can be shifted by the drain–source bias. Since IGZO is a classic ETL and HBL, holes drift to the NiO source efficiently without injecting into the IGZO drain. On the other hand, even though the negative gate voltage increases the IGZO/QD interface

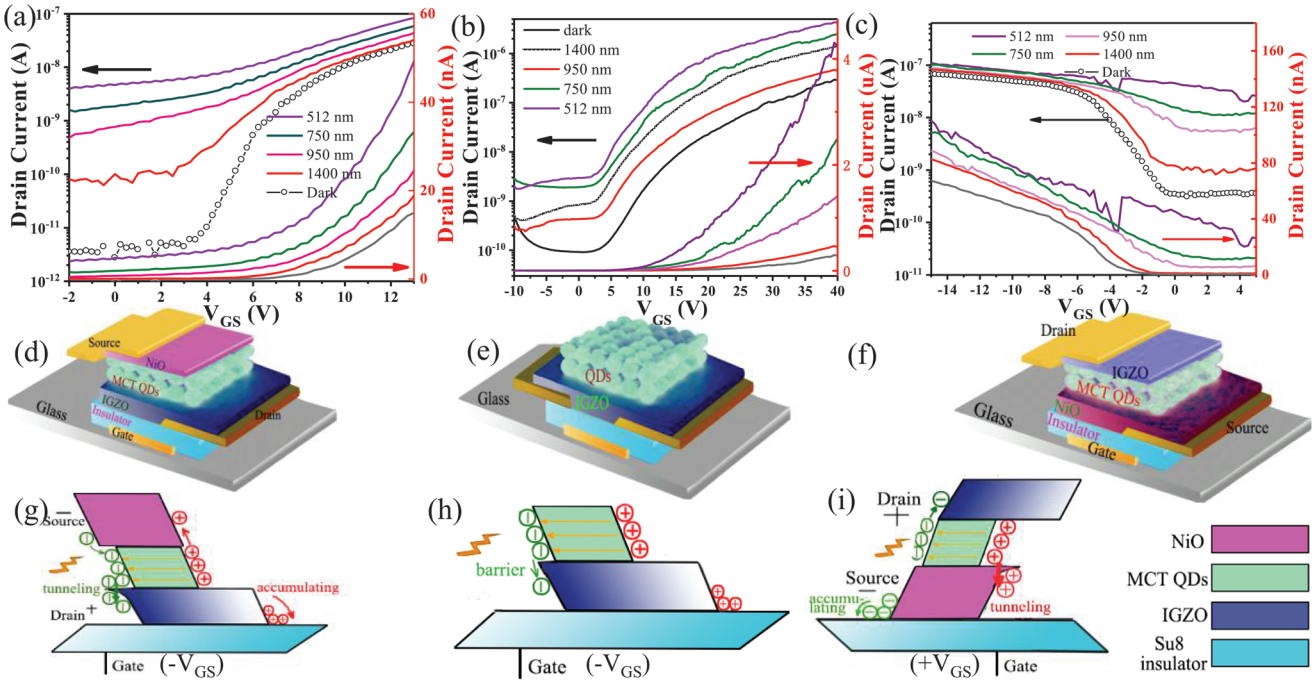

Figure 4. Transfer characteristic curves of the PIN phototransistor (V_{DS} = 1 V) a), QD-IGZO PT (V_{DS} = 3 V) b) and the P-PIN phototransistor (V_{DS} = 2 V) c) illuminated by incident light with different wavelengths (light power = 5 pW). Schematics of the compared PIN d), QD-IGZO e) and P-PIN f) phototransistors' structures. Panels (g)–(i) are the photocarrier generation and transport for these different devices, respectively.

barrier height, the electrons can tunnel into the IGZO drain due to the barrier becoming narrower with increasing electron accumulation at the interface. For the positive gate regime, two possible origins are considered for these enhancements: 1) in the on-gate regime, the photodetector generally has a very unclear photocurrent gain in the absence of electric rectification; 2) the efficiencies of extracting photoexcited electrons and holes are very low because of NiO and IGZO blocking the extractions, respectively.

The corresponding conventional QD/IGZO PT needs the built-in potential to extract electrons from the QDs to the IGZO active layer, requiring a higher gate voltage and intensive light bias. Considering both the above-described carrier lifetime analysis and the photoresponse experiments, the PIN heterostructure increases the photocarrier extraction and transportation efficiency compared to those of the conventional QD/IGZO PT. Encouraged by the successful fabrication and verification of the PIN phototransistor, the inverted structure NiO/QD/IGZO PIN phototransistor (because it shows p-type transfer IV character, we defined as P-PIN phototransistor) was also produced, and its optoelectric properties were measured to establish the model of the PIN phototransistor. Our electrical measurements shows that the effective carriers modulated in this device are holes, as can be demonstrated in the transfer characteristic curves (positive gate off-regime and negative gate on-regime) presented in Figure 4c. One interesting phenomenon is that the P-PIN phototransistor shows a remarkable photocurrent gain at the positive gate voltage under illumination, in agreement with our previous hypothesis for the charge tunneling in the heterostructure (as observed in Figure 4f,i). Besides, the two vertical structures phototransistors show more zig-zag IV characters (Figure 4a,c) compared with planar counterpart (Figure 4b), because QD is the main and direct composition of the vertical channel. It can result in more drain–source current's noise (it usually comes from dark current's tunneling and injection, charge's trapping in the defects and more photothermal noise's influence).

The investigation of the position-dependent photoresponse of the phototransistor is very valuable for understand the photosensing behavior. Using a high-power microscope (Leica DM4000), DPS/DMS microregion laser system and motorized positioning stages, position- and spectrum-dependent photocurrent mapping was performed to investigate and characterize the static optoelectric performances of the as-designed devices. As shown in **Figure 5**a, the size of the laser spot can be decreased by the objective lens to generate high resolution photocurrent information within the device. The phototransistor shows intense photoresponse and small current corrugation under illumination on the heterostructure region containing the gate's active zone. The photoresponse decreased at the channel and nearly vanished at the capped source area, as shown in Figure 5c. To summarize, coupling of the gate bias and heterostructure is the key factor for obtaining a highly efficient photoresponse.

Figure 5b shows the spectra photocurrent responsivity and efficiency (EQE = $R \cdot h\nu/q$) corresponding to the continuous spectrum laser sources and current sampling system, where R is the responsivity ($R = I_{ph}/P_{in}$, I_{ph} is the photocurrent and P_{in} is the incident light power), q is the electronic charge, q is Plank's constant, and ν is the frequency of the incident photon. The extreme responsivity and EQE of the PIN phototransistor can reach approximately 10^3 A W^{-1} and 10^3%, respectively, which are slightly higher than the corresponding values for the P-PIN and

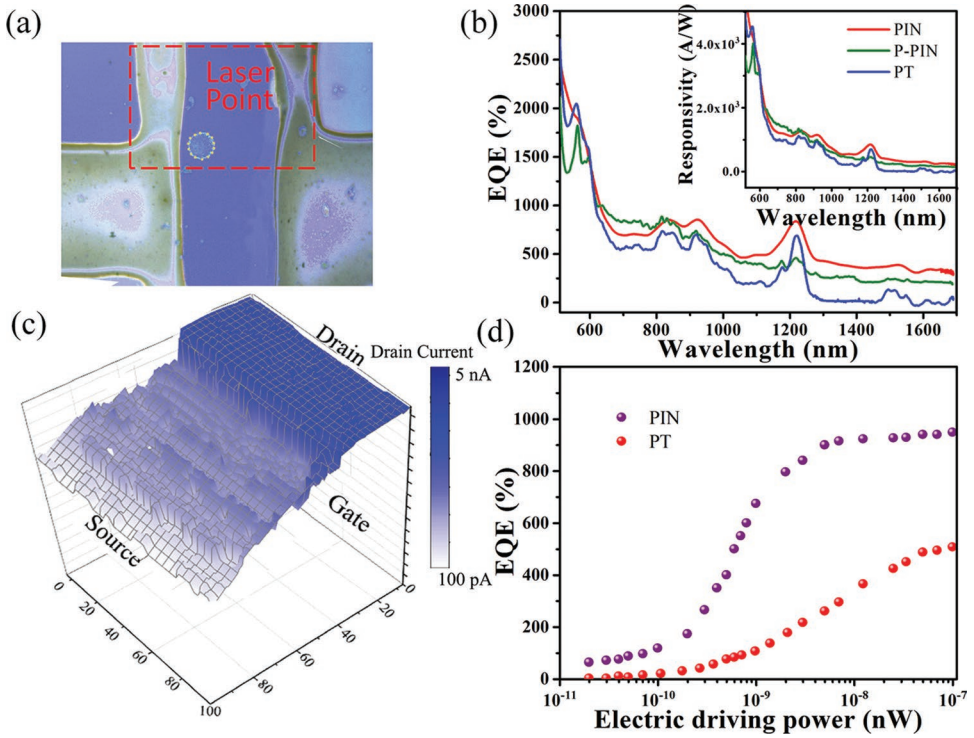

Figure 5. a) Illustration of the device's photocurrent mapping processes using our measurement systems. b) The EQE trend-line along the incident light's wavelengths ($V_{GS} = -2$ V, $V_{DS} = 1$ V). c) The measured position-dependent photocurrent for this PIN phototransistor's channel by 1.5 μm IR laser illumination ($V_{GS} = -2$ V, $V_{DS} = 1$ V, light power = 10 pW). d) The EQE versus electrical driving drain–source terminal power.

conventional PT devices due to the abovementioned enhancement. This high photoelectrical gain can be explained through microcosmic and macroscopic analysis: 1) the photoconductive gain can be determined by photosensing QD's recombination lifetime (τ_0) and transit time ($\tau_{tr} = L \cdot W/(\mu \cdot V_{DS})$),[33,34] which is given by gain = τ_0/τ_{tr}. Because this vertical structure has very short vertical transfer channel ($L \approx 100$ nm, $W = 1$ mm) and relative high mobility of IGZO (25 $cm^2 V^{-1} S$), the transit time is on the order of 4 ps. It leads to a photoelectrical gain of around 50 times, using previous measured 0.2 ns carrier's lifetime (Figure 1), in good agreement with measured EQE gain. 2) The photogating effect is commonly observed in phototransistor, which can amplify both the dark current and photocurrent.[35] As shown in **Figure 6**a, the gate voltage exhibits vital function to generate enough photosignal, which can produce extra induced charges in the channel. Consequently, the drain–source voltage bias can provide extra energy and photocurrent without changing the incident light's intensity.

Furthermore, the exotic properties of the PIN heterostructure make it a promising candidate for use as a low-power photodetector that has a factor of 10 lower power supply requirement for the same EQE compared with conventional PT (Figure 5d). By operating at a subthreshold driving drain voltage ($V_{DS} \leq 1$ V), the PIN phototransistor can obtain nearly 500% at an electrical driving power of 1 nW. As a consequence, a possible strategy to reduce the working power can also improve the optoelectric efficiency by engineering an effective heterostructure for the oxide thin film transistors.

The PPC effect from oxygen vacancies is the main question that has stymied the development of zinc-oxide phototransistors for direct photodetection applications.[36,37] The excellent repeatability and immediate photoresponse in dynamic IR detection are important advantages for the actual application of the integrated phototransistor. The obtained photocurrent signals of the compared devices with different gate voltages are shown in Figure 6a. The photocurrent response time is affected by the devices' structures due to the photocarrier generation mechanism. The photoelectrons generated from the QDs rapidly (recovery time < 100 ms) tunnel through the QD/IGZO barrier with the negative gate voltage. Nevertheless, conventional IGZO-based PT suffers from the PPC effect with a very slow recovery time (≈20 s), because it must form a positive hole inversion layer and maintain V_O^{2+} positive charges for a long time. Notably, the photocurrent attenuation displayed in Figure 6b provides empirical evidence to suggest that 1) the as-prepared conventional IGZO/QD PT clearly has a very low detection bandwidth (<0.5 Hz) at −3 dB decay; 2) the PIN phototransistor's bandwidth (201 Hz) is higher than that of its P-PIN counterpart because electrons are much more flexible and light than holes. Meanwhile, direct printing IGZO on the Su8 insulator for this PIN phototransistor has much better surface quality than printing on the rough QD/NiO substrate with less interstitial and trap states within the heterostructure interface.

Finally, the other important figure of merit of a photodetector is the detectivity. It is useful to calculate the detectivity of the present devices for comparison with the values reported in the literature, particularly under dynamic detecting circumstances. The detectivity D^* is the ability of the sensor to detect a weak signal. It characterizes the sensor relative to its noise, which

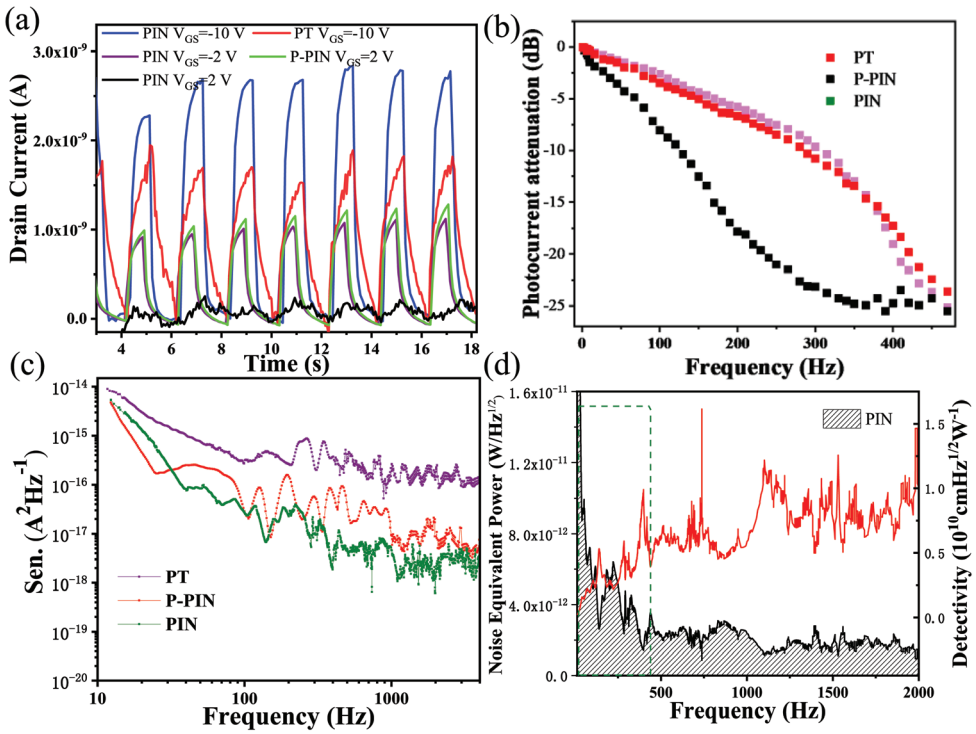

Figure 6. a) Light signal response (1.5 µm; peak power = 10 pW) comparison for the devices under different gate voltages. b) Photocurrent damping curves versus detection frequency under infrared 1.5 µm illumination. c) Noise spectral density (Sen.) of the phototransistors with different heterostructures (V_{GS} = –10 V, V_{DS} = 1 V), under ambient conditions at room temperature. d) Noise equivalent power (NEP) and detectivity spectrum of the optimized PIN phototransistor versus the gate frequency under a dynamic detecting environment of 200 Hz.

can be determined from the above noise current spectrum. The detectivity is given by the following[38,39]

$$\mathrm{NEP} = \frac{I_N}{R}\left(\mathrm{wHz}^{-1/2}\right) \quad D^* = \frac{\sqrt{A}}{\mathrm{NEP}}\left(\mathrm{cm\,Hz^{1/2}\,w^{-1}, Jones}\right) \tag{1}$$

where NEP is the noise-equivalent power, A is the active area, I_N is the noise current density, and R is the responsivity.

The detectivity of the PIN phototransistor is found at the level of the lowest noise current density due to the low dark current and longer diffusion length in the heterostructures (as shown in Figure 6c). The PIN phototransistor's ultimate dynamic performances can be derived and are presented in Figure 6d. The spectrum analyzer measurement bandwidth can be estimated by the formula $\int_0^\infty \mathrm{NEP}(f)\mathrm{d}(f) = \mathrm{NEP}(f)\Delta f$. Experimentally, the obtained modulation bandwidth is similar to the previously measured signal bandwidth values, indicating the influence of the contacted interface within the channel. Further exploration and improvement should be focused on optimization of the film's quality and interface matching. Moreover, this IR phototransistor simultaneously achieves 1×10^{11} cm Hz$^{1/2}$ W^{-1} detectivity under a dynamic detecting environment, which is comparable to the values for the commercial compound IR photodetectors.

In summary, multiterminal optoelectronic measurements, photoresponse, EQE, XPS, PL, and bandwidth/detectivity characterizations provided strong evidence that high detection performances and excellent electronic properties can be achieved for the PIN phototransistor via the fabrication of our heterostructure. Due to rectifying behavior and photocarrier extracting enhancement, it is highly likely that an optimal balance of the detector properties, such as detection efficiency, driving power and speed, can be obtained by using this nonphotolithographic method systematically. This method can be applied not only for photosensitive materials but also to open prospects for achieving cost-effective and integrated photodetector devices.

Acknowledgements

The authors acknowledge funding from the National Natural Science Foundation of China (Grant No: 61905116). The authors also acknowledge financial support from the Natural Science Foundation of Jiangsu Province (BK20190771) and the Natural Science Foundation of the Jiangsu Higher Education Institutions of China (16KJB510020). This work was also supported by the Science and Technology innovation project of Nanjing for overseas returnees (R2019LZ01).

Conflict of Interest

The authors declare no conflict of interest.

Keywords

infrared photodetectors, narrow-band phototransistors, printing process, QD-based PIN heterostructures

[1] X. Yu, T. J. Marks, A. Facchetti, *Nat. Mater.* **2016**, *15*, 383.
[2] J. Yu, K. Javaid, L. Liang, W. Wu, Y. Liang, A. Song, H. Zhang, W. Shi, T. C. Chang, H. Cao, *ACS Appl. Mater. Interfaces* **2018**, *10*, 8102.
[3] D. K. Hwang, Y. T. Lee, H. S. Lee, J. L. Yun, S. H. Shokouh, J. Kyhm, J. Lee, H. K. Hong, T. H. Yoo, S. H. Nam, *NPG Asia Mater.* **2016**, *8*, e233.
[4] M. Sun, Q. Fang, Z. Zhang, D. Xie, Y. Sun, J. Xu, W. Li, T. Ren, Y. Zhang, *ACS Appl. Mater. Interfaces* **2018**, *10*, 7231.
[5] H. Hosono, *Nat. Electron.* **2018**, *1*, 428.
[6] T. Cramer, I. Fratelli, P. Barquinha, A. Santa, C. Fernandes, F. D'Annunzio, C. Loussert, R. Martins, E. Fortunato, B. Fraboni, *Sci. Adv.* **2018**, *4*, eaat1825.
[7] L. Li, L. Gu, Z. Lou, Z. Fan, G. Shen, *ACS Nano* **2017**, *11*, 4067.
[8] Y. Zang, F. Zhang, D. Huang, X. Gao, C. A. Di, D. Zhu, *Nat. Commun.* **2015**, *6*, 6269.
[9] S. Rim, Y. M. Yang, S. H. Bae, H. Chen, C. Li, M. S. Goorsky, Y. Yang, *Adv. Mater.* **2015**, *27*, 6885.
[10] J. J. Gough, N. Mcevoy, M. O'Brien, A. P. Bell, D. Mccloskey, J. B. Boland, J. N. Coleman, G. S. Duesberg, A. L. Bradley, *Adv. Funct. Mater.* **2018**, *28*, 1706149.
[11] M. Gong, R. Sakidja, Q. Liu, R. Goul, E. Dan, M. Casper, A. Stramel, A. Elliot, J. Z. Wu, *Adv. Opt. Mater.* **2018**, *6*, 1701241.
[12] S. Knobelspies, A. Daus, G. Cantarella, L. Petti, G. A. Salvatore, *Adv. Electron. Mater.* **2016**, *2*, 1600273.
[13] J. Zhang, M. Zhang, C. Du, S. Zhang, L. Zhang, *IEEE Electron Device Lett.* **2019**, *40*, 1.
[14] Z. Pei, H. C. Lai, J. Y. Wang, W. H. Chiang, C. H. Chen, *IEEE Electron Device Lett.* **2014**, *36*, 44.
[15] H. Xue, Y. Dai, W. Kim, Y. Wang, Z. Sun, *Nanoscale* **2019**, *11*, 3240.
[16] Y. Dai, X. Wang, W. Peng, C. Xu, C. Wu, K. Dong, R. Liu, Z. L. Wang, *Adv. Mater.* **2018**, *30*, 1705893.
[17] J. W. Lee, D. Y. Kim, F. So, *Adv. Funct. Mater.* **2015**, *25*, 1233.
[18] J. Lu, X. Sheng, G. Tong, Z. Yu, X. Sun, L. Yu, X. Xu, J. Wang, J. Xu, Y. Shi, K. Chen, *Adv. Mater.* **2017**, *29*, 1700400.
[19] D. C. Perng, H. P. Lin, M. H. Hong, *Appl. Phys. Lett.* **2015**, *107*, 241113.
[20] S. Lee, A. Nathan, *Science* **2016**, *354*, 302.
[21] Y. Liu, H. Zhou, R. Cheng, W. Yu, Y. Huang, X. Duan, *Nano Lett.* **2014**, *14*, 1413.
[22] S. Kim, Y. J. Choi, Y. Choi, M. S. Kang, J. H. Cho, *Adv. Funct. Mater.* **2017**, *27*, 1700651.
[23] X. Liu, X. Yang, M. Liu, Z. Tao, Q. Dai, L. Wei, C. Li, X. Zhang, B. Wang, A. Nathan, *Appl. Phys. Lett.* **2014**, *104*, 113501.
[24] X. Liu, W. Kuang, H. Ni, Z. Tao, Q. Huang, J. Chen, Q. Liu, J. Chang, W. Lei, *Nanoscale* **2018**, *10*, 10182.
[25] W. E. Tennant, M. Thomas, L. J. Kozlowski, W. V. Mclevige, D. D. Edwall, M. Zandian, K. Spariosu, G. Hildebrand, V. Gil, P. Ely, *J. Electron. Mater.* **2001**, *30*, 590.
[26] N. Huo, S. Gupta, G. Konstantatos, *Adv. Mater.* **2017**, *29*, 1606576.
[27] M. Chen, H. Lu, N. M. Abdelazim, Y. Zhu, Z. Wang, W. Ren, S. V. Kershaw, A. L. Rogach, N. Zhao, *ACS Nano* **2017**, *11*, 5614.
[28] L. Wang, S. Chen, W. Li, K. Wang, Z. Lou, G. Shen, *Adv. Mater.* **2019**, *31*, 1804583.
[29] D. W. Kim, K. Cho, H. Kim, B. M. Moon, S. Kim, *Microelectron. Eng.* **2007**, *84*, 1643.
[30] A. L. Rogach, M. T. Harrison, S. V. Kershaw, A. Kornowski, M. G. Burt, A. Eychmüller, H. Weller, *Phys. Status Solidi B* **2001**, *224*, 153.
[31] R. Cheng, W. Feng, Y. Lei, X. Kai, J. He, *Appl. Phys. Lett.* **2017**, *110*, 173507.
[32] X. Liu, Y. Chen, D. Li, S. W. Wang, H. C. Kuo, *Photonics Res.* **2019**, *7*, 311.
[33] J. Y. Wu, Y. T. Chun, S. Li, T. Zhang, J. Wang, P. K. Shrestha, D. Chu, *Adv. Mater.* **2018**, *30*, 1705880.
[34] Y. U. Yu, Y. Zhang, L. Jin, Z. Chen, L. I. Yifan, L. I. Qingyan, M. Cao, Y. Che, H. Dai, J. Yang, *Photonics Res.* **2019**, *7*, 149.
[35] H. Fang, W. Hu, *Adv. Sci.* **2017**, *4*, 1700323.
[36] B. Ryu, H.-K. Noh, E.-A. Choi, K. J. Chang, *Appl. Phys. Lett.* **2010**, *97*, 022108.
[37] S. Jeon, S. E. Ahn, I. Song, C. J. Kim, U. I. Chung, E. Lee, I. Yoo, A. Nathan, S. Lee, J. Robertson, K. Kim, *Nat. Mater.* **2012**, *11*, 301.
[38] X. Liu, L. Gu, Q. Zhang, J. Wu, Y. Long, Z. Fan, *Nat. Commun.* **2014**, *5*, 4007.
[39] K. A. Sablon, A. Sergeev, S. Najmaei, M. Dubey, *Nanophotonics* **2017**, *6*, 1263.